CLUH regulates mitochondrial biogenesis by binding mRNAs of nuclear-encoded mitochondrial proteins

Jie Gao,[1,2] Désirée Schatton,[1] Paola Martinelli,[1] Henriette Hansen,[1] David Pla-Martin,[1] Esther Barth,[1] Christian Becker,[3] Janine Altmueller,[3] Peter Frommolt,[4] Marco Sardiello,[5,6] and Elena I. Rugarli[1,2,4]

[1]Institute for Genetics, [2]Center for Molecular Medicine, [3]Cologne Center for Genomics, and [4]Cologne Excellence Cluster on Cellular Stress Responses in Aging-Associated Diseases, University of Cologne, 50923 Cologne, Germany
[5]Department of Molecular and Human Genetics, Baylor College of Medicine, Houston, TX 77030
[6]Jan and Dan Duncan Neurological Research Institute, Texas Children's Hospital, Houston, TX 77030

Mitochondrial function requires coordination of two genomes for protein biogenesis, efficient quality control mechanisms, and appropriate distribution of the organelles within the cell. How these mechanisms are integrated is currently not understood. Loss of the Clu1/CluA homologue (*CLUH*) gene led to clustering of the mitochondrial network by an unknown mechanism. We find that *CLUH* is coregulated both with genes encoding mitochondrial proteins and with genes involved in ribosomal biogenesis and translation. Our functional analysis identifies CLUH as a cytosolic messenger ribonucleic acid (RNA; mRNA)–binding protein. RNA immunoprecipitation experiments followed by next-generation sequencing demonstrated that CLUH specifically binds a subset of mRNAs encoding mitochondrial proteins. CLUH depletion decreased the levels of proteins translated by target transcripts and caused mitochondrial clustering. A fraction of CLUH colocalizes with tyrosinated tubulin and can be detected close to mitochondria, suggesting a role in regulating transport or translation of target transcripts close to mitochondria. Our data unravel a novel mechanism linking mitochondrial biogenesis and distribution.

Introduction

Mitochondrial homeostasis depends on effective biogenesis, quality control mechanisms, and appropriate distribution of the mitochondrial network and is key to cell survival. Dysfunctional mitochondria can trigger apoptotic cell death and play an important role in the pathogenesis of several diseases (Nunnari and Suomalainen, 2012). The interplay between mitochondrial distribution and biogenesis is still largely unexplored. Most mitochondrial proteins are encoded in the nucleus, translated in the cytosol, and subsequently imported into the mitochondrion. However, it is poorly understood whether mitochondrial biogenesis involves a specific subcellular localization of mRNAs for nuclear-encoded mitochondrial proteins.

The CluA protein was first identified in *Dictyostelium discoideum* as a determinant of mitochondrial distribution in cells (Zhu et al., 1997). Disruption of the CluA gene led to clustering of mitochondria near the nucleus and to multinucleated cells. Ultrastructural analysis showed the presence of thin connections between the clustered mitochondria, hinting to a defect in late phases of mitochondrial fission (Fields et al., 2002). CluA gene homologues have been described in several species. In yeast and plant, deletion of the orthologous gene led to mitochondrial clustering and did not affect cell division (Fields et al., 1998; Logan et al., 2003). *Drosophila melanogaster clueless* deletion mutants were characterized by small size, lack of motor coordination, sterility, and short life span and displayed signs of flight muscle defect (Cox and Spradling, 2009). Mitochondria in affected muscles appeared swollen and showed vesiculation or loss of cristae.

Correspondence to Elena I. Rugarli: Elena.Rugarli@uni-koeln.de

Abbreviations used in this paper: CLIP, cross-linking immunoprecipitation; FC, fold change; GSEA, gene set enrichment analysis; KO, knockout; MEF, mouse embryonic fibroblast; mol wt, molecular weight; MT, microtubule; PNK, polynucleotide kinase; RAP, ribosomal-associated protein; RBP, RNA-binding protein; RIP, RNA immunoprecipitation.

The Rockefeller University Press $30.00
J. Cell Biol. Vol. 207 No. 2 213–223
www.jcb.org/cgi/doi/10.1083/jcb.201403129

Moreover, mitochondria clustered in the female germ cells at the sites of microtubule (MT) plus ends and remained clustered during mitosis in early germ cells, suggesting unequal inheritance in the absence of *clu* (Cox and Spradling, 2009). Adult Clu mutants showed drastically reduced ATP levels and signs of oxidative damage (Sen et al., 2013). Based on these data, it was proposed that Clu has a role in positioning mitochondria within the cell based on their physiological status.

We now show that the mammalian CLUH is an RNA-binding protein (RBP), which specifically binds a subset of mRNAs for nuclear-encoded mitochondrial proteins. CLUH depletion leads to mitochondrial clustering and reduced steady-state levels of proteins encoded by target mRNAs, indicating that CLUH links mitochondrial biogenesis and distribution.

Results and discussion

CLUH is coregulated with genes encoding mitochondrial proteins and involved in translation

Despite high evolutionary conservation (Fig. S1, A and B), the function of CLUH is still unknown. Coexpression analysis is a powerful tool to identify candidate pathways in which a gene is involved. We performed a systems biology analysis of the *CLUH* gene regulatory network by analyzing thousands of publicly available expression microarray experiments representative of multiple tissues and conditions after chemical, biological, or genetic perturbation (Sardiello et al., 2009; Gennarino et al., 2011). Strikingly, these analyses showed that human and mouse *CLUH* are significantly coexpressed with genes involved in mitochondrial metabolic pathways and oxidative phosphorylation and, surprisingly, also with genes that participate in cytosolic ribosomal biogenesis, RNA processing, and translation (Figs. 1 A and S1 C). Genes encoding for mitochondrial proteins and genes involved in the biogenesis of RNP complexes form two partially overlapping clusters in the *Cluh* gene regulatory network (Fig. 1 B) and occupy high-ranking positions within the *Cluh* coregulation list (Fig. S1 C). Gene set enrichment analysis (GSEA) shows that these two sets of genes have a skewed distribution in the list of mouse genes when it is ranked by degree of coregulation with *Cluh*: genes encoding for mitochondrial proteins and genes involved in ribosome biogenesis tend to occupy high-ranking positions within the list (enrichment scores = 0.55 for mitochondrion and 0.64 for ribosome biogenesis; $P < 10^{-4}$ for all analyses; Fig. 1, C and D). These data strongly support the connection of CLUH with mitochondrial biogenesis and suggest a role of CLUH in the regulation of translation.

CLUH exists in cytosolic granules that partially associate with tyrosinated tubulin and mitochondria

In *Drosophila*, Clu formed cytosolic aggregates that sometimes associated with MTs and were found next to mitochondria (Cox and Spradling, 2009). In COS7 cells, endogenous CLUH showed a granular cytosolic signal, which substantially decreased after CLUH depletion by RNAi (Fig. 2, A and B). We found poor colocalization of CLUH with β-tubulin and acetylated tubulin, a marker of old stable MTs (Fig. S2, A–F). In contrast, CLUH granules showed significant colocalization with tyrosinated tubulin, which labels newly assembled MTs (Fig. 2, C–F). Colocalization was maintained also after disruption of MTs by nocodazole, suggesting that this interaction does not depend on intact MT tracks but rather on the presence of soluble tubulin α/β heterodimers (Fig. S2, G–I). Consistently, CLUH did not associate with taxol-stabilized MT bundles or with MT tracks after detergent extraction of soluble proteins before fixation (Fig. S2, J–O). However, upon this treatment, the pattern of CLUH staining strikingly changed and was reminiscent of an organellar structure (Fig. 2, G and K; and Fig. S2, M–O). Labeling of these structures using an antibody against a mitochondrial marker demonstrated that under this condition, CLUH decorates mitochondria (Fig. 2, K–N). Similar results were obtained upon overexpression of a tagged version of CLUH (Fig. S2, P–U). Although we cannot rule out an artificial change of CLUH localization upon detergent extraction, it is conceivable that a fraction of CLUH residing in close proximity to mitochondria is revealed only after extraction of soluble CLUH or other interacting proteins.

Next, we performed sequential cell fractionation experiments. In mouse brain and liver, CLUH was detected in the crude mitochondrial fraction and the cytosol but was mostly enriched in a light membrane fraction (Fig. 2 O). Because the yeast Clu1p was previously identified as one of the subunit of the eIF3 eukaryotic translation factor (Vornlocher et al., 1999), we concentrated ribosomes and ribosomal-associated proteins (RAPs) by differential centrifugation (Otto et al., 2005). CLUH was detected in the pellet containing ribosomes and RAPs and was released in the supernatant by high salt washes, similar to EIF3G (Fig. 2 P). This crude purification does not allow conclusive establishment of CLUH association with the translation initiation machinery. We therefore investigated the distribution of CLUH in polysome profiles obtained in HeLa cells. As expected, EIF3G was enriched in the fractions corresponding to the 40S subunit. CLUH was mainly detected in lighter fractions containing free RNAs (Fig. 2 Q), indicating that it exists in a large part independently from the ribosomes. More experiments will be required to ascertain whether CLUH might be recruited to the eIF3 complex under specific conditions.

CLUH deficiency impairs mitochondrial distribution in mammalian cells

To assess whether lack of CLUH leads to a mitochondrial phenotype in mammalian cells, we depleted the protein using RNAi in COS7 cells. We observed that a significant percentage of cells showed abnormalities of mitochondrial distribution and morphology. The mitochondrial network lost its tubular appearance and collapsed on one side of the nucleus (Fig. 3, A and B). Despite their abnormal distribution, mitochondria possessed normal ultrastructure and conservation of the cristae structure (Fig. 3 C). We did not observe connections between clustered mitochondria that were previously described in *D. discoideum* (Fields et al., 2002). Mitochondrial clustering and neurite retraction were observed after depleting CLUH in NSC34 cells, a motoneuronal cell line (Fig. S3, A–D). Neurite retraction is

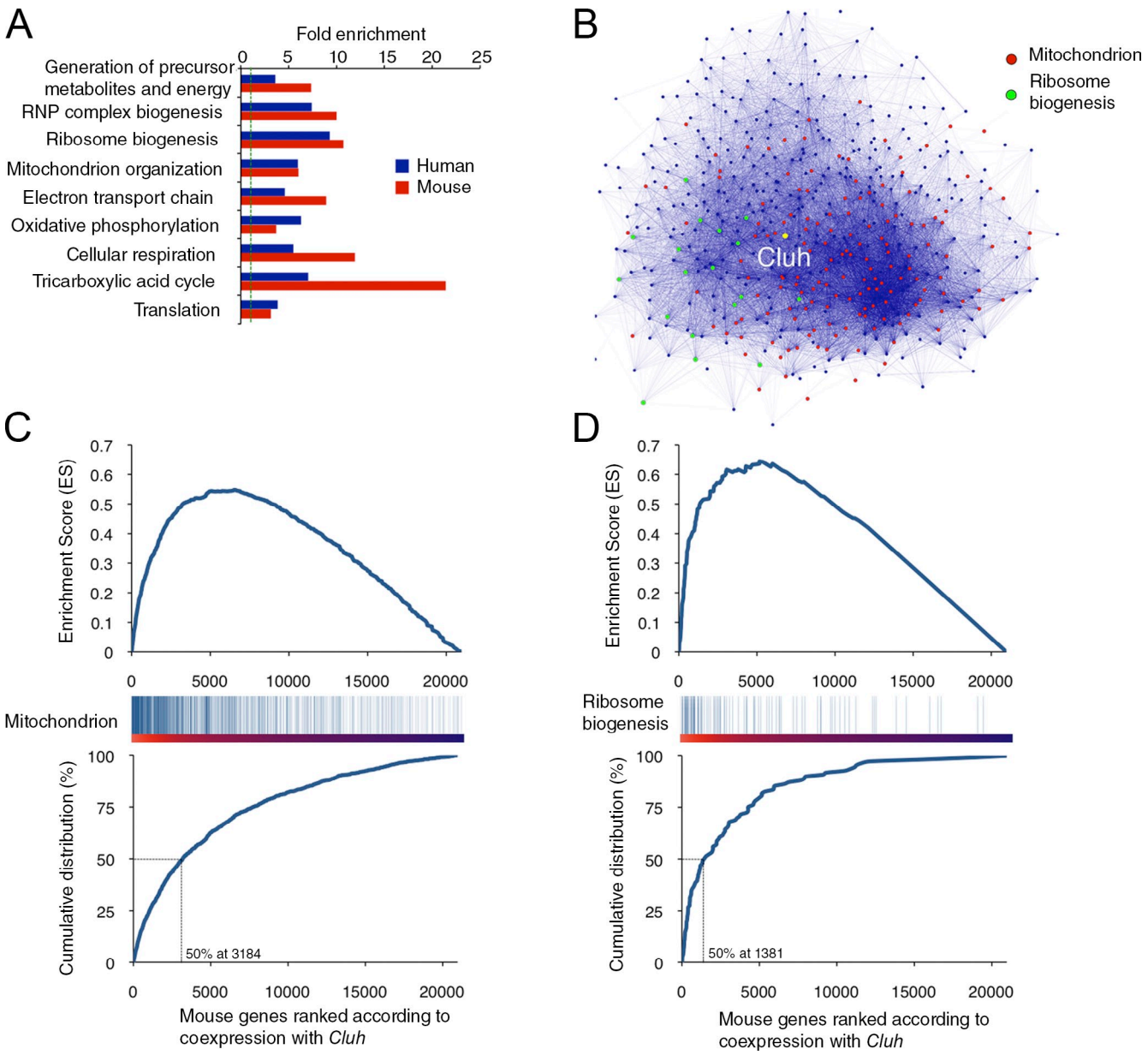

Figure 1. **Coregulation analysis of *CLUH*.** (A) Gene Ontology analysis of the network of genes that are coexpressed with *CLUH*/*Cluh*. The fold enrichment for the biological process Gene Ontology terms is shown ($P < 10^{-4}$). The green dotted line corresponds to fold enrichment of 1. (B) Cytoscape-generated *Cluh* gene regulatory network. Genes encoding mitochondrial- and ribosomal biogenesis–related proteins are highlighted and are connected by blue lines whose color intensity is proportional to the extent of their coregulation. (C and D) GSEA of *Cluh* regulatory network for mitochondrion genes (C) and ribosome biogenesis genes (D). The x axis shows the rank for the first 20,000 genes in the coregulation list. The graphs on the top display the enrichment scores. Middle panels show enrichment plots, in which the relative positions of genes are indicated as vertical blue bars (left, most similar expression to *Cluh* [red]; right, less similar expression to *Cluh* [blue]). The graphs on the bottom show the cumulative distribution of the gene sets within the ranked lists. 50% of mitochondrion and ribosome biogenesis gene sets are found in the first ∼15 and 7% of *Cluh* coregulation list, respectively.

consistent with mitochondria depletion from axons and dendrites, as previously observed (van Spronsen et al., 2013).

We also generated mouse embryonic fibroblasts (MEFs) deficient for *Cluh*. These cells did not show any overt defect in cell growth or difference in mitochondrial mass measured by FACS after labeling the organelles with MitoTracker green (Fig. 3 D). However, analysis of their mitochondrial network showed aggregated mitochondria, which were detected as less numerous and with higher area/perimeter by automatic quantification (Fig. 3, E–G).

CLUH is an RBP and binds mRNAs of nuclear-encoded mitochondrial proteins

To integrate our previous findings into a functional model, we postulated that CLUH regulates biogenesis of nuclear-encoded mitochondrial proteins by binding their mRNAs. To test this hypothesis, we performed cross-linking immunoprecipitation (CLIP) experiments (Jensen and Darnell, 2008). HeLa cells were exposed to UV irradiation to generate a covalent bond between RNA–protein complexes. After partial hydrolysis of the RNA, the RNA–protein complex was immunoprecipitated with

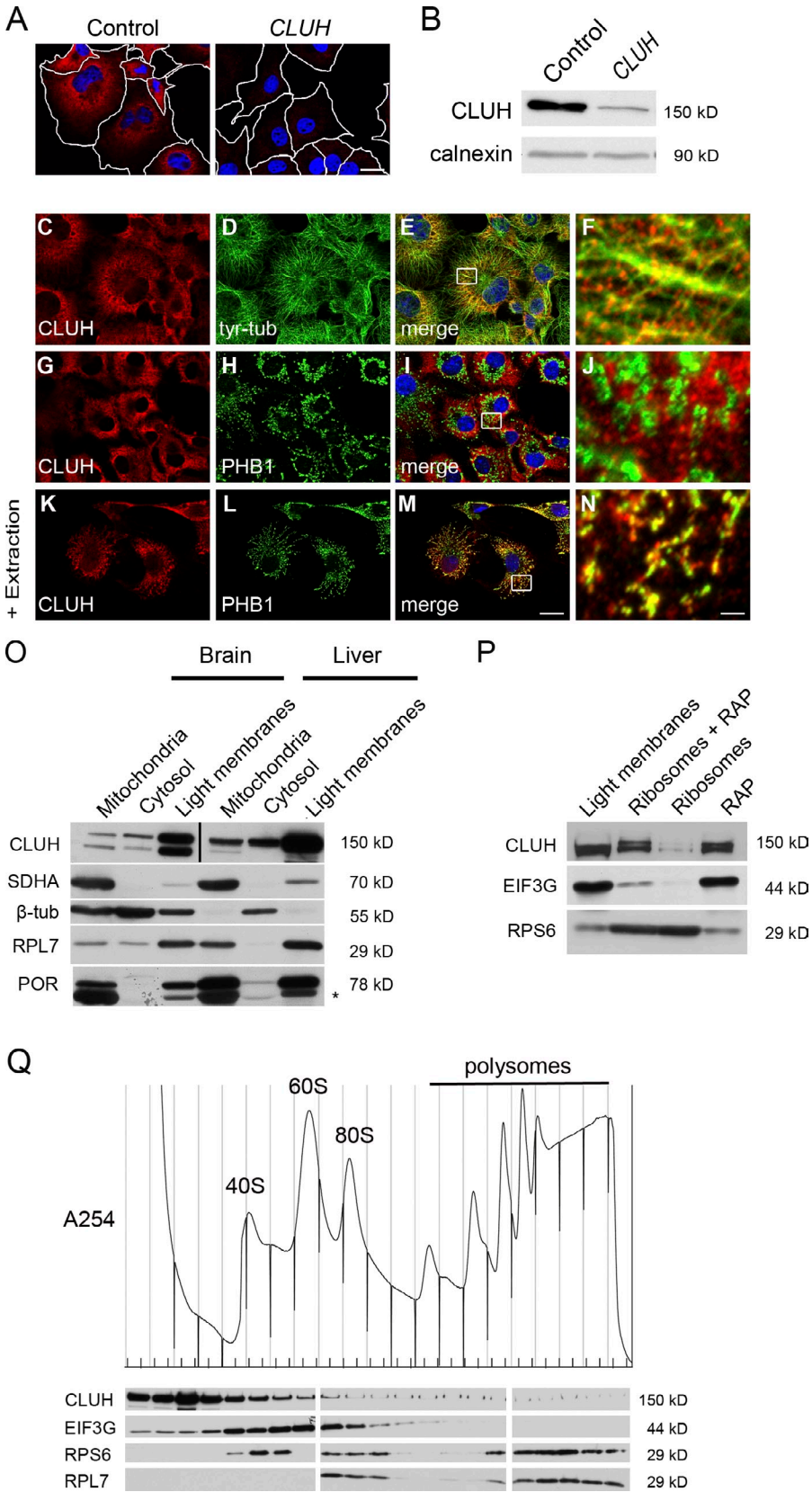

Figure 2. **Subcellular localization of CLUH.** (A and B) Endogenous CLUH signal can be efficiently depleted by RNAi in COS7 cells. White lines indicate the border of the cells. (C–F) CLUH partially colocalizes with tyrosinated tubulin (tyr-tub). (G–N) After Triton X-100 extraction of soluble proteins, CLUH subcellular pattern changes (compare G with K and J with N), and CLUH decorates mitochondria labeled with an antibody against prohibitin (PHB1; N). F, J, and N show enlarged boxed regions. (O) Subcellular fractionation of murine brain and liver. Asterisk indicates leftover signal from SDHA. The black line indicates that intervening lanes have been spliced out. POR, cytochrome P450 reductase. (P) Liver light membranes were sedimented through a sucrose gradient to obtain a pellet enriched for ribosomes and RAPs. This pellet was resuspended in a high-salt buffer and further centrifuged to release RAPs (supernatant) from ribosomes (pellet). (Q) Polysome profiles in HeLa cells. UV absorbance of the fractions is shown on the top, and the corresponding Western blots are shown on the bottom. Bars: (A, C–E, G–I, and K–M) 20 µm; (F, J, and N) 2.5 µm.

the anti-CLUH antibody followed by RNA end labeling with γ-[^{32}P]ATP. The radioactive complex was then separated by SDS-PAGE. Autoradiography showed a radiolabeled RNA–protein complex at the expected molecular weight (mol wt) of CLUH only after UV cross-linking. This complex shifted to a higher mol wt when lower concentrations of RNase were used (Fig. 4 A).

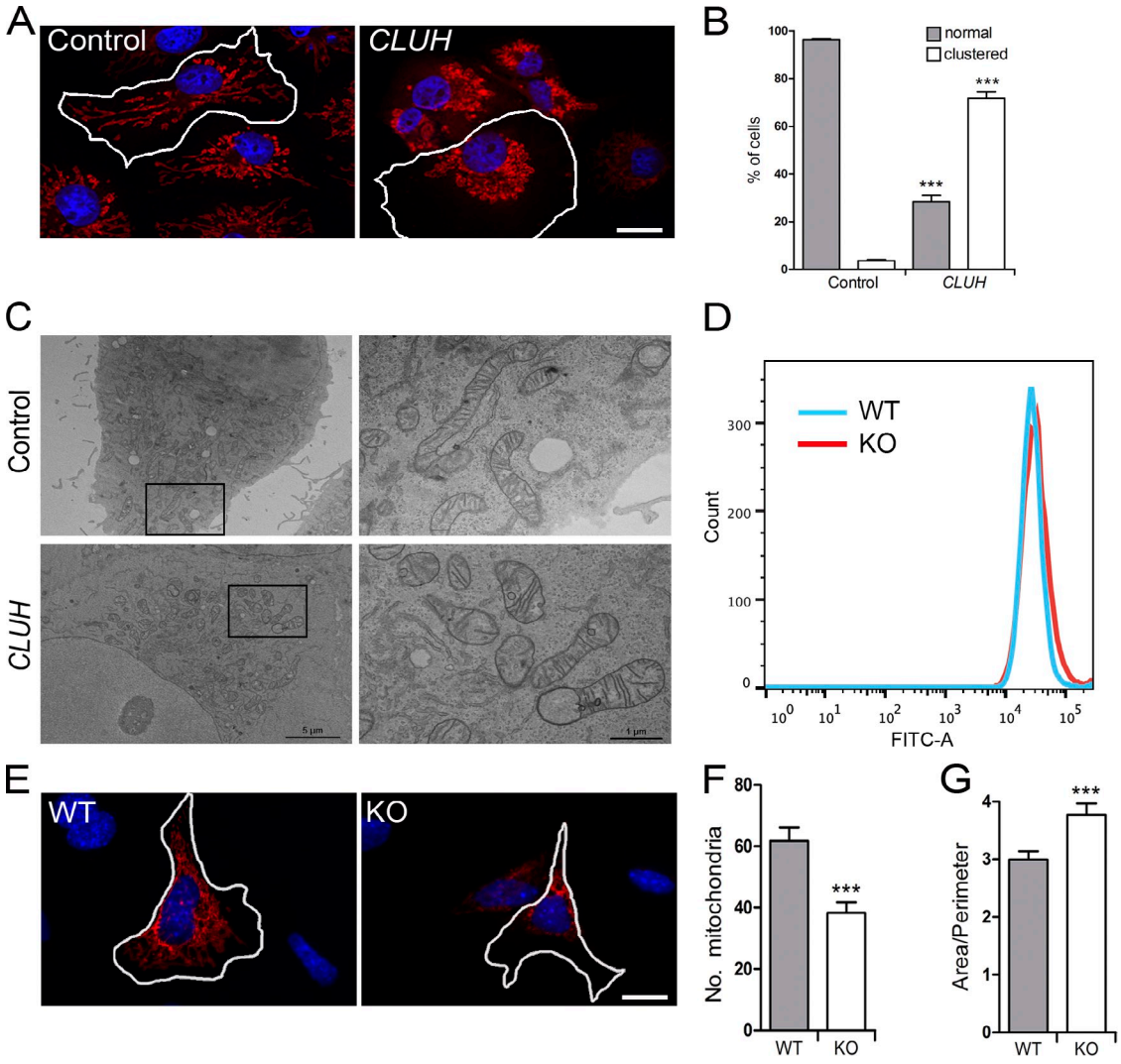

Figure 3. **CLUH depletion induces mitochondrial clustering.** (A) COS7 cells were silenced with *CLUH*-specific or control siRNA. Mitochondria were stained with MitoTracker red. White lines indicate the border of the cell. (B) Quantification of mitochondrial clustering phenotype in COS7 cells. 300–400 cells were counted per experiment (n = 3). (C) Electron micrograph of representative COS7 cells. Right images show higher magnification of boxed areas. (D) FACS analysis of mitochondrial mass in MEFs. The x axis shows the log scale of the fluorescence intensity of the peaks. FITC-A, FITC area mode. One representative experiment out of three is shown. (E) Mitochondrial distribution in wild-type and *Cluh*-deficient MEFs transfected with mito-mCherry. (F and G) Quantification of mitochondrial profiles with ImageJ. At least 50 cells were analyzed per experiment (n = 3). ***, $P \leq 0.001$. Bars: (A and E) 20 µm. Error bars show standard errors of the mean. WT, wild type.

No band was detected in CLIP experiments using a control IgG (anti-AFG3L1).

To obtain an independent evidence of CLUH acting as an RBP, we constructed a stable HEK 293T cell line overexpressing tetracycline-inducible CLUH-FLAG. The CLIP experiment was repeated using the anti-FLAG antibody either in cells overexpressing CLUH or an empty vector, confirming that CLUH directly binds mRNAs (Fig. 4 B). Despite the fact that CLUH does not possess a known RNA-binding domain, our data are consistent with recent systematic studies in HeLa cells and yeast (Castello et al., 2012; Mitchell et al., 2013).

To identify the CLUH target mRNAs in an unbiased and genome-wide manner, we performed next-generation sequencing on three independent RNA immunoprecipitation (RIP) experiments after UV cross-linking in HeLa cells using the CLUH antibody or the control IgG. Library quality control is summarized in Table S1. 259 transcripts displayed a fold enrichment greater than five in the CLUH-RIP versus the IgG-RIP samples with a $P < 0.01$ (Table S3). Remarkably, 234 of these mRNAs are annotated as mitochondrial proteins. We obtained similar results when we compared the enrichment of transcripts found in the CLUH-RIP samples to the input HeLa transcriptome (Table S4). 233 mRNAs were common to both comparisons using the same cutoff values (Table S5). Analysis of these transcripts with Ingenuity confirmed a striking enrichment of canonical pathways and diseases and function annotations related to mitochondria (Fig. 4 C). To further confirm these data, we selected a few CLUH target transcripts and performed quantitative RT-PCR analyses in independent RIP experiments. We found consistent enrichment for *ATP5A1*, *SPG7*, *OPA1*, *OGDH*, and *GOT2* mRNAs in CLUH-RIP versus IgG-RIP samples, in contrast to control mRNAs (Fig. 4 D). Interestingly, many of the CLUH-bound transcripts

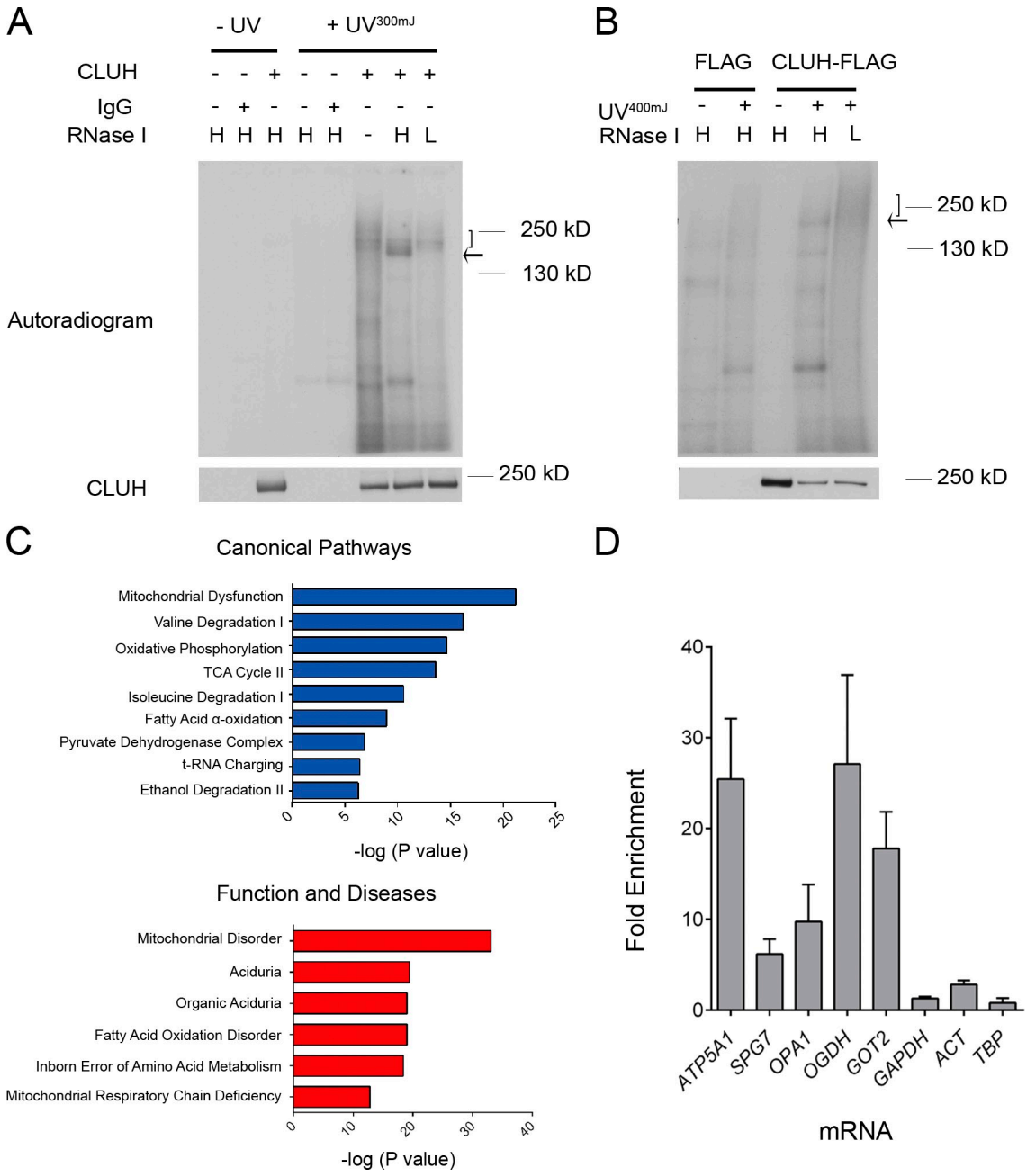

Figure 4. **CLUH is an RBP and binds to mRNAs encoding mitochondrial proteins.** (A) Autoradiogram of CLIP experiment in HeLa cells using the indicated antibodies. An RNA–protein complex of the expected size is visible upon UV cross-linking (arrow) and is shifted to a higher mol wt smear (bracket) when a lower concentration of RNase was applied. H, high RNase concentration; L, low RNase concentration. The bottom shows the corresponding Western blot. (B) Autoradiogram of CLIP experiment in HEK 293T cells expressing either an empty vector or a CLUH-FLAG construct. An RNA–protein complex of the expected size is visible upon UV cross-linking and is shifted to a higher mol wt by reducing the concentration of RNase. The bottom shows the corresponding Western blot. (C) Transcripts enriched more than fivefold ($P < 0.01$) in CLUH-RIP compared with IgG-RIP. Samples were analyzed by Ingenuity Pathway Analysis. Bars indicate the p-value for the most significant pathways and function and disease annotations. (D) Fold enrichment of transcripts immunoprecipitated by the CLUH versus the IgG antibody measured by quantitative RT-PCR ($n = 3–5$). Error bars show standard errors of the mean.

were also present in the coregulation list, consistent with a common transcriptional program regulating both CLUH and its targets. These data establish that CLUH specifically binds mRNAs of a subset of nuclear-encoded mitochondrial proteins.

CLUH depletion decreases the levels of proteins encoded by target mRNAs

RBPs can affect any aspect of RNA life, including RNA stability, transport, and translation efficiency. First, we excluded that CLUH deletion globally affects cytosolic translation rates in knockout (KO) MEFs or down-regulated NSC34 cells (Figs. 5 A and S3 E). Consistently, polysome profiling did not show obvious differences in *Cluh*-deficient compared with control cells (Figs. 5 B and S3 F). We then asked whether the levels of CLUH target mRNAs or encoded proteins were affected by *Cluh* deficiency (Fig. 5, C–F; and Fig. S3, G and H). We analyzed genes that were proven to be CLUH targets in RIP experiments (*Atp5a1*, *Opa1*, *Ogdh*, *Got2*, *Spg7*, *Pdha*, and *Sdha*), and

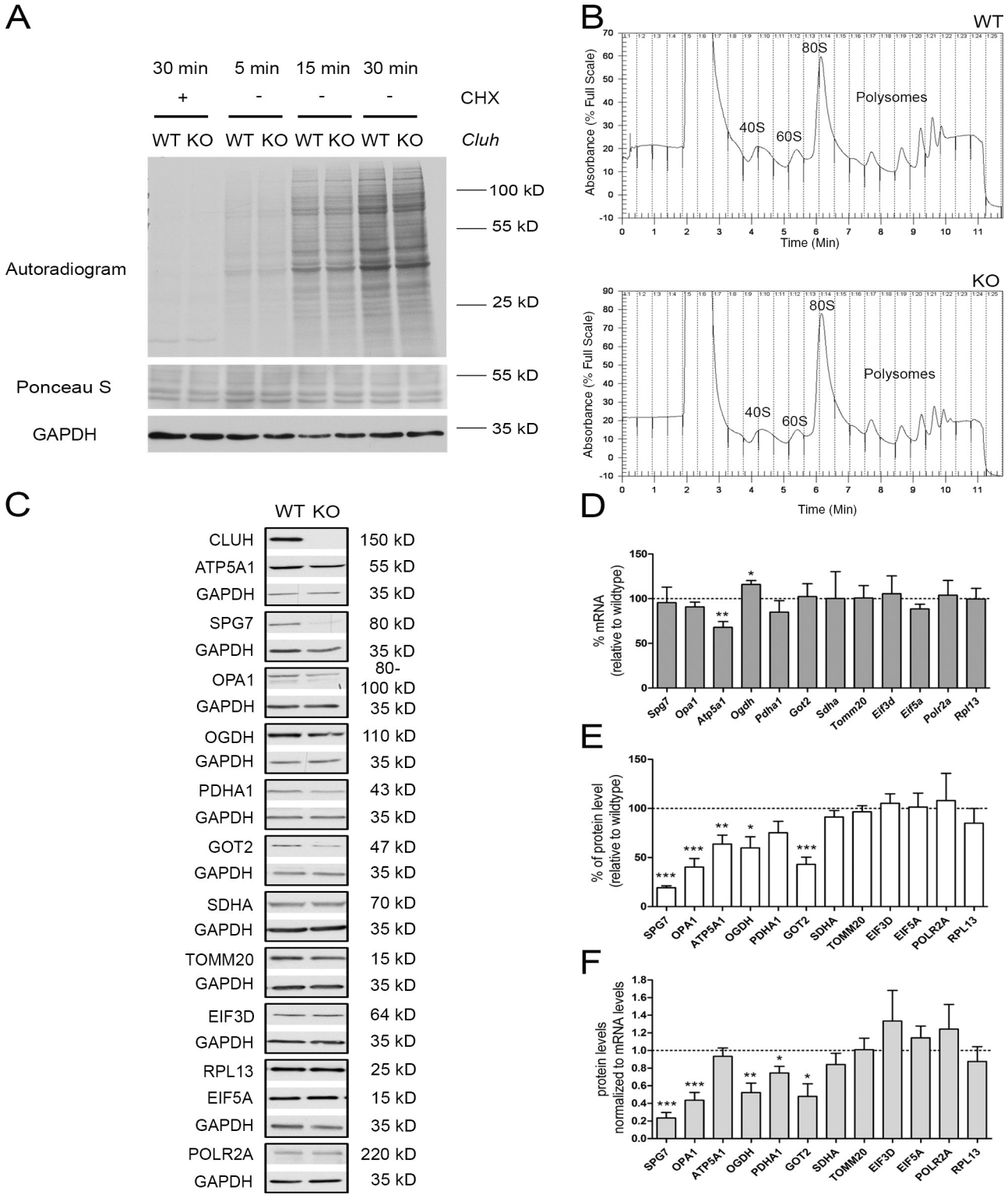

Figure 5. **CLUH depletion decreases levels of proteins encoded by target mRNAs.** (A) *Cluh* KO does not affect the general translation rate in MEFs. CHX, cycloheximide. (B) Polysome profiling of *Cluh* KO MEFs does not show an obvious difference compared with that obtained in wild-type (WT) cells. This experiment has been completed once. (C) Western blots of WT and KO MEFs were decorated with antibodies against proteins encoded by CLUH target and control transcripts. (D) Quantitative RT-PCR of CLUH target and control transcripts in *Cluh* KO MEFs. The level of each transcript is expressed as a ratio to GAPDH ($n = 4$). (E) Quantification of Western blots shown in C ($n = 4$). (F) Protein levels in E were normalized to RNA levels in D. ***, $P \leq 0.001$; **, $P \leq 0.01$; *, $P \leq 0.05$. Error bars show standard errors of the mean.

as a control, genes that were not significantly enriched (including genes encoding the mitochondrial protein TOMM20 and ribosomal or eukaryotic initiation factor components found in the coregulation list). Only the transcript level of *Atp5a1* was significantly reduced in *Cluh* KO MEFs, providing a possible explanation for the reduced steady-state levels of the protein detected by Western blotting (Fig. 5 C). In contrast, we observed a significant decrease of the protein levels when normalized to the mRNA levels of SPG7, OPA1, OGDH, PDHA1, and GOT2 in CLUH-deficient cells. SDHA showed a tendency toward a reduction, whereas all control genes were unaffected (Fig. 5, C–F). Our data are also consistent with decreased levels of pyruvate dehydrogenase and complex V α subunit previously reported in flies lacking Clu (Cox and Spradling, 2009).

In conclusion, we demonstrate that CLUH is a novel RBP that specifically binds a subset of mRNAs for nuclear-encoded mitochondrial proteins, thus playing a previously unrecognized role in mitochondrial biogenesis. Pathway enrichment analysis of CLUH target transcripts and the coexpression data strongly reinforce the hypothesis that CLUH is required to support a specific program of mitochondrial biogenesis. Target CLUH transcripts encode not only for components of the respiratory chain but also for molecules involved in the TCA cycle and in fatty acid and amino acid metabolism. Moreover, CLUH binds the mRNA encoding for PINK1 (Tables S3–S5), a mitochondrial protein kinase involved in Parkinson disease and shown to act upstream of parkin (Clark et al., 2006; Park et al., 2006; Narendra and Youle, 2011). This result could provide an explanation for the genetic interaction between Clu and parkin previously observed in *Drosophila* (Cox and Spradling, 2009).

Ad hoc experiments are now necessary to understand whether CLUH regulates stability, transport, and/or translation of its target mRNAs. Both in yeast and mammalian cells, a subset of mRNAs encoding for mitochondrial proteins was asymmetrically localized to the vicinity of the organelle (Marc et al., 2002; Margeot et al., 2002; Devaux et al., 2010; Matsumoto et al., 2012). The localization of mRNAs to a particular subcellular compartment leads to efficient translation of proteins next to the location where they are needed. Such a process allows for fast temporal and spatial regulation of gene expression and protects the cell from possible toxic effects caused by protein mistargeting (Martin and Ephrussi, 2009). Furthermore, cells may need to quickly regulate translation of mitochondrial proteins, depending on their metabolic status, for example, changes of substrate availability.

Down-regulation of CLUH in mammalian cells alters mitochondrial distribution, as previously shown in other species (Zhu et al., 1997; Fields et al., 1998; Logan et al., 2003; Cox and Spradling, 2009). Mitochondrial clustering has been observed upon mitochondrial fragmentation, loss of mitochondrial membrane potential preceding mitophagy, and disruption of anterograde movement of mitochondria (Tanaka et al., 1998; Smirnova et al., 2001; Cho et al., 2007; Lee et al., 2010). It is conceivable that alteration in mitochondrial distribution observed in *Cluh*-depleted cells is secondary to a defect in mitochondrial biogenesis. Alternatively, CLUH might regulate both mitochondrial and RNP movement via yet-unknown interactors. A hint for an active role of CLUH in transport of RNPs comes from the partial association of CLUH with tyrosinated tubulin, which labels newly assembled MTs and MT plus ends. The identification of CLUH as the first mammalian RBP that binds mRNAs for nuclear-encoded mitochondrial proteins sheds a completely new light on the function of this highly conserved protein and opens novel avenues of research to elucidate mechanisms of regulation of mitochondrial biogenesis.

Materials and methods

Coregulation analysis

GSEA was performed as previously described (Subramanian et al., 2005). In brief, the lists of genes belonging to the mitochondrion and the ribosome biogenesis groups were downloaded from the Gene Ontology database, and the GSEA tool was used to evaluate their distribution within a genome-wide list of genes that were ranked according to their degree of coexpression with *Cluh*. The cumulative distribution function was constructed by performing 1,000 random gene set membership assignments. A nominal $P < 0.01$ and a false discovery rate of <10% were used to assess the significance of the enrichment score. Gene Ontology analyses were performed with the webtool DAVID (Database for Annotation, Visualization and Integrated Discovery; Huang et al., 2009) using default parameters. The *Cluh* gene network was obtained by performing pathway coexpression analyses as previously described (Gennarino et al., 2011; Song et al., 2013). In brief, *Cluh* was used as a bait to analyze a vast set of transcriptional profiles available at the Gene Expression Omnibus database (Barrett et al., 2007). Multiple cellular conditions and tissues are represented in this database. To ensure data homogeneity, the analysis was focused on experiments that used the Mouse Genome 430 2.0 Array (GeneChip; Affymetrix). For each gene represented in the Affymetrix platform, a pairwise coexpression score with *Cluh* was calculated as its cumulative occurrence in the top 3% of correlated genes across all investigated experiments (Gennarino et al., 2011; Song et al., 2013). The expression correlation data were then analyzed with Cytoscape (Lopes et al., 2010) to draw a visual representation of expression relationships among genes. Genes annotated as mitochondrion and ribosome biogenesis in DAVID were highlighted in the Cytoscape-generated network by using different color codes.

Generation and culture of cell lines

Cluh$^{loxP/loxP}$-conditional mice were generated by conventional gene targeting in C57BL6/N embryonic stem cells using constructs designed to insert intronic *LoxP* sites flanking exon 10 of mouse *Cluh*. *Cluh*$^{loxP/loxP}$ animals were crossed with cytomegalovirus-Cre transgenic mice to generate *Cluh*$^{+/-}$ heterozygous mice. Primary fibroblasts were isolated from embryonic day 14.5 embryos derived from a mating between *Cluh*$^{+/-}$ mice and immortalized using a plasmid encoding SV40 large T antigen. All animal procedures were performed according to protocols approved by the Institutional Animal Care and Use Committee.

MEFs, HeLa, and COS7 cells were cultured in DMEM supplemented with 10% FetalClone III serum (Thermo Fisher Scientific), 2% penicillin-streptomycin (Life Technologies), and 2 mM L-glutamine (Life Technologies). NSC34 cells (Cashman et al., 1992) were cultured in DMEM, supplemented with 5% defined FBS (Thermo Fisher Scientific), 2% penicillin-streptomycin, and 2 mM L-glutamine.

RNAi and neurite quantification

NSC34 or COS7 cells were grown to 70–80% confluence. Predesigned siRNAs against murine *Cluh* (oligonucleotide [oligo] 1, 5′-CAUGGACCGUGAGGAUACUUGUCAU-3′; oligo 2, 5′-CCUCGGUCAUGCUGUUGAAUGGUGA-3′; and oligo 3, 5′-CCGAAUCCAUGUGCGUCAUGUCAGA-3′) or human *CLUH* (oligo 1, 5′-UCCUUCCUCCUUGGAGUCCAAGUCU-3′; oligo 2, 5′-CCACCAGCUGGACCACGUCUUUAAA-3′; and oligo 3, 5′-AACACCAGCAGCAUGAGGUAGCGGG-3′) were obtained from Life Technologies and transfected individually or together in a 1:1:1 ratio using Lipofectamine 2000 (Life Technologies) with a final concentration of 100 nM. For immunofluorescence staining, cells were plated on coverslips after 48 h of down-regulation, and immunofluorescence experiments were performed after an additional 24 h. For cell lysate preparation, cells were harvested 72 h after transfection and lysed with buffer containing 50 mM Tris-HCl, pH 7.4, 150 mM NaCl, 1 mM EDTA, pH 8, 1% IGEPAL CA-630, 0.25% sodium deoxycholate, and protease inhibitor cocktail (Sigma-Aldrich).

Neurite length was measured with AxioVision version 4.8 2.0 (Carl Zeiss). 150–500 cells were analyzed per experiment, and neurite length was categorized as longer or shorter than 30 µm.

Immunofluorescence and imaging

Cells were washed twice with PBS and fixed with 4% paraformaldehyde, pH 7.4, in PBS for 30 min at RT or with ice-cold methanol for 20 min at −20°C. Cells were permeabilized with 0.2% Triton X-100 in PBS for 10 min, blocked in 10% pig serum in PBS for 10 min, and subjected to primary antibodies diluted in PBS including 1% pig serum for 2 h at RT. PEM extraction of soluble proteins was performed as described before (Cappelletti et al., 2003). In brief, cells were washed twice with PEM buffer (85 mM Pipes, pH 6.94, 10 mM EGTA, 1 mM $MgCl_2$, 2 M glycerol, and 1 mM PMSF supplemented with protease inhibitor cocktail), and soluble proteins were extracted by incubating cells for 10 min with PEM buffer including 0.1% Triton X-100 at RT. Cells were fixed with ice-cold methanol for 10 min at −20°C followed by standard immunofluorescence protocol. Primary antibodies were diluted as follows: polyclonal rabbit CLUH at 1:1,000 (Novus Biologicals), monoclonal mouse prohibitin at 1:100 (Neo Markers), monoclonal mouse tyrosinated tubulin at 1:400, monoclonal mouse α-tubulin at 1:500, monoclonal mouse β-tubulin at 1:500, monoclonal mouse acetylated tubulin at 1:100, and polyclonal rabbit FLAG at 1:100 (Sigma-Aldrich). Subsequently, coverslips were washed in PBS and incubated in secondary antibodies, swine α-rabbit TRITC (Dako) diluted 1:200 and goat α-mouse Alexa Fluor 488 (Life Technologies) diluted 1:500 in PBS including 1% pig serum for 1 h at RT. MitoTracker red CMXRos (Life Technologies) staining was performed according to the manufacturer's instructions. Coverslips were washed twice with PBS, mounted with Fluorsave (EMD Millipore), and visualized with an epifluorescence microscope (Imager.M2m; Carl Zeiss) mounting an ApoTome module (Carl Zeiss) and a 63×, 1.4 NA oil immersion objective lens (Plan Apochromat; Carl Zeiss) at RT. Images were acquired using a camera (AxioCam MRm; Carl Zeiss) and the software AxioVision version 4.8.2.0 (Carl Zeiss). Images represent a single plane with a thickness of 0.250 µm.

Quantification of mitochondrial mass and morphology

To measure mitochondrial content in MEFs, 100,000 cells were seeded on 30-mm dishes. 24 h later, cells were trypsinized, washed with PBS, and loaded with 200 nM MitoTracker green fluorescent mitochondrial (Life Technologies) in complete medium for 25 min. Cells were then washed twice with PBS and resuspended with PBS containing 1% FetalClone III serum before analysis with a cell sorter (FACS Aria III; BD). Experiments were performed three times (10,000 events in each replicate). Mitochondrial morphology in COS7 and NSC34 cells was scored by an experimenter who was blind to the genotype. Mitochondria were labeled either with MitoTracker red CMXRos or by transfection with mito-mCherry. Mitochondrial area/perimeter and number of particles in MEFs were obtained using ImageJ (National Institutes of Health), using a macro developed by Dagda et al. (2009). The image analysis macro can be downloaded at the following link: http://imagejdocu.tudor.lu/doku.php?id=plugin:morphology:mitochondrial_morphology_macro_plug-in:start.

Electron microscopy

COS7 were prepared for electron microscopy, as previously described (Wakabayashi et al., 2009). In brief, cells were fixed for 1 h in prewarmed 2% (vol/vol) glutaraldehyde, 2.5% (mol wt/vol) sucrose, 3 mM $CaCl_2$, and 100 mM Hepes-KOH, pH 7.4. After washes, cells were postfixed using reduced OsO_4 (1% [mol wt/vol] OsO_4, 10 mg/ml potassium ferrocyanide, 1.25% [mol wt/vol] sucrose, and 100 mM sodium cacodylate, pH 7.4) for 1 h on ice. Cells were then incubated in 2% (mol wt/vol) uranyl acetate for 30 min. After dehydration using 50, 70, 90, and 100% ethanol, samples were embedded in Epon (Fluka). Samples were observed under a transmission electron microscope (EM 902; Carl Zeiss) at an acceleration voltage of 80 kV, and micrographs were acquired using a camera (MegaView 3; Olympus).

Cell fractionation experiments

Mouse tissues were homogenized in 220 mM mannitol, 70 mM sucrose, 20 mM Hepes-NaOH, pH 7.4, 1 mM EDTA, and 0.1% BSA. Large debris were eliminated by centrifugation at 500 *g* at 4°C for 10 min, and the supernatant was centrifuged again at 1,000 *g* to remove the nuclear fraction. Mitochondria were obtained by centrifugation at 8,000 *g* for 10 min. The resulting supernatant was then centrifuged at 20,000 *g* for 10 min followed by ultracentrifugation at 170,000 *g* for 45 min. Light membranes were harvested by dissolving the pellet in buffer containing 50 mM Tris-HCl, pH 7.4, 150 mM NaCl, 1 mM EDTA, pH 8, 1% IGEPAL CA-630, 0.25% sodium deoxycholate, and protease inhibitor cocktail. The protein concentration was measured with Bio-Rad Protein Assay (Bio-Rad Laboratories), and 40 µg protein was loaded for each fraction.

For preparation of RAPs, mouse liver was homogenized in 250 mM sucrose, 20 mM Hepes-KOH, pH 7.4, 5 mM $MgCl_2$, 50 mM K-acetate, 1 mM DTT, and 1 mM PMSF. Postmitochondrial supernatant was obtained by centrifugation at 17,000 *g*. Light membranes were prepared by centrifugation at 100,000 *g* for 3 h. Two parts of the membrane fraction were then layered onto one part of sucrose cushion containing 1 M sucrose, 20 mM Tris-HCl, pH 7.5, 2 mM $MgCl_2$, 0.1 mM EDTA, and 500 mM KCl and centrifuged at 275,000 *g* for 2.5 h. The pellet was then resuspended in 500 mM sucrose, 50 mM Tris-HCl, pH 7.5, 1 mM DTT, 0.1 mM EDTA, and 700 mM KCl followed by centrifugation at 200,000 *g* for 1.5 h to separate the RAPs (supernatant) and ribosomes (pellet). 50 µg of each fraction was loaded onto SDS-PAGE for analysis.

Sucrose gradient and polysome profiling

Cells were harvested at 70–80% of confluence. Polysomes were stalled by treating the cells with 100 µg/ml cycloheximide (Sigma-Aldrich) for 15 min. Cells were washed and scraped in PBS containing cycloheximide at 4°C. After pelleting cells at 21,000 *g* for 15 s, the pellet was lysed in buffer containing 20 mM Tris-HCl, pH 7.4, 30 mM KCl, 0.5% Triton X-100, 2 mM DTT, 1 mg/ml heparin, 100 µg/ml cycloheximide, and 0.16 U/ml RNase inhibitor (RNasin Plus; Promega). The lysates were then loaded onto a 7–47% (mol wt/vol) continuous sucrose gradient and centrifuged at 97,658 *g* for 3 h at 4°C in a rotor (SW41; Beckman Coulter). For polysome profiling, fractions were monitored at 254 nm using a UA-6 detector and collected with a density gradient fractionation system (Foxy R1 Fraction Collector; Teledyne ISCO). For Western blot analysis, the same volume of samples from each fraction was loaded on the SDS-PAGE.

Western blot analysis and quantification

The following antibodies were used: polyclonal rabbit CLUH (detecting human and mouse CLUH), polyclonal rabbit RPL7, polyclonal rabbit RPS6, polyclonal rabbit EIF3G, polyclonal rabbit EIF3D, and polyclonal rabbit POLR2A obtained from Novus Biologicals; monoclonal mouse GAPDH and monoclonal mouse panactin obtained from EMD Millipore; monoclonal mouse ATP5A1 and monoclonal mouse SDHA obtained from Life Technologies; monoclonal mouse OPA1 purchased from BD; monoclonal mouse PDHA1, monoclonal rabbit GOT2, polyclonal rabbit OGDH, polyclonal rabbit EIF5A, monoclonal rabbit RPL13, monoclonal mouse ATP5A1, and polyclonal rabbit OPA1 purchased from Abcam; polyclonal rabbit TOMM20 obtained from Santa Cruz Biotechnology, Inc.; monoclonal mouse β-tubulin obtained from Sigma-Aldrich; polyclonal rabbit calnexin obtained from Biotrend; and polyclonal rabbit cytochrome P450 reductase obtained from Stressgen. The polyclonal rabbit antibody against paraplegin was produced using as antigen a His-tagged fusion protein containing amino acids 50–307 of mouse paraplegin (Ferreirinha et al., 2004). Quantification of Western blots was performed with ImageJ ($n = 4$).

Generation of the CLUH-FLAG overexpression cell line

The full-length cDNA of human *CLUH* was cloned into the p3×FLAG-CMV-14 (Sigma-Aldrich). Stable transfected cells were obtained using the Flp-In T-REx 293 cell system (Life Technologies). The cells were maintained in DMEM (Life Technologies), 7.5% tetracycline-free FBS (Biochrom AG), 1 mM sodium pyruvate (Life Technologies), nonessential amino acids (Life Technologies), 2 mM L-glutamine and 1.5 mg/ml hygromycin (InvivoGen), and 150 µg/ml blasticidin (InvivoGen). 1 µg/ml tetracycline (dissolved in ethanol) was used to induce protein expression.

CLIP and RIP

Cells were harvested at 70–80% of confluence. HeLa and HEK 293T cells were cross-linked with 300 and 400 mJ/cm^2, respectively (CX2000 UV cross-linker; UVP). After collection, the cell pellet was lysed in cold lysis buffer (50 mM Tris-HCl, pH 7.4, 100 mM NaCl, 1 mM $MgCl_2$, 0.1 mM $CaCl_2$, 1% IGEPAL CA-630, 0.1% SDS, and 0.5% sodium deoxycholate) supplemented with different concentrations of RNase I (Life Technologies; 50 U/500 µl lysate or 1 U/500 µl lysate) and 4 U TURBO DNase (Life Technologies) per 500 µl cell lysate. The cleared lysate was then incubated with 0.5 µg anti-CLUH (Novus Biologicals), 0.5 µg anti-AFG3L1 (Koppen et al., 2007), no antibody, or 3 µg anti-FLAG (Sigma-Aldrich) for 1 h at 4°C with head-to-toe rotation. The complex was immunoprecipitated by the addition of 20 µl protein G Dynabeads (Life Technologies) for 1 h at

4°C. The beads were then washed extensively with lysis buffer followed by high salt buffer (50 mM Tris-HCl, pH 7.4, 1 M NaCl, 1% IGEPAL CA-630, 0.1% SDS, 0.5% sodium deoxycholate, and 1 mM EDTA) and primed with T4 polynucleotide kinase (PNK) buffer (20 mM Tris-HCl, pH 7.4, 10 mM $MgCl_2$, and 0.2% Tween 20). RNA end labeling was performed by incubating the beads with PNK buffer (New England Biolabs, Inc.), 2 µl T4 PNK (20 U; New England Biolabs, Inc.), and 1 µl γ-[^{32}P]ATP (10 mCi/ml; PerkinElmer) at 37°C for 5 min with agitation. The beads were then washed first with PNK buffer plus 20 mM EGTA and then with high salt buffer. The RNP complex was then released by incubating the beads with lithium dodecyl sulfate sample buffer (Bolt; Life Technologies) and reducing agent (Bolt) at 70°C for 10 min with agitation. The samples were resolved onto 4–12% minigel (Bolt). The gel was dried and exposed to obtain the autoradiograph.

RIP and RIP-seq

For RIP, the procedure was the same as described in the previous paragraph, except that no RNase I was added to the lysis buffer. Libraries were prepared using the RNA sample preparation kit (TruSeq v2; Illumina). Starting material was 1 µg total RNA from the input samples, and complete material of the RIP experiments (240–550 ng RIP RNA). After poly-A selection (using poly-T oligo–attached magnetic beads), mRNA was purified and fragmented using divalent cations under elevated temperature. The RNA fragments underwent reverse transcription using random primers. This is followed by second-strand cDNA synthesis with DNA Polymerase I and RNase H. After end repair and A tailing, indexing adapters were ligated. The products were then purified and amplified (15 PCR cycles) to create the final cDNA libraries. After validation (2200 TapeStation; Agilent Technologies) and quantification (Qubit System; Invitrogen), the pool was quantified by using the KAPA Library Quantification kit (Peqlab) and the 7900HT Sequence Detection System (Applied Biosystems). The pool was loaded on a sequencer (MiSeq; Illumina) and sequenced with a 2 × 76–bp v3 protocol.

Data were analyzed using a high-throughput next-generation sequencing analysis pipeline: Basic read quality check was performed using FastQC (Babraham Bioinformatics) and read statistics were obtained with SAMtools. Reads were mapped to the human reference assembly, version GRCh37, using TopHat2 (Kim et al., 2013), and gene quantification was performed using a combination of Cufflinks (Trapnell et al., 2010) and the DEseq2 package (Anders and Huber, 2010) with genomic annotation from the Ensembl database, version 75. The results were uploaded into an in-house MySQL database and merged with annotations obtained with biomaRt from Ensembl, version 75. The gene lists were filtered according to fold change (FC) and p-value in comparison of the library size-normalized read counts between samples and controls. The sample and control means as well as FC and p-values (Tables S3 and S4, columns B–E) were calculated with the DESeq2 package from the Bioconductor project. Wald's test was used for significance testing. In contrast, gene expression for the individual samples was calculated by the Cufflinks package (Table S3 and S4, columns F–Q) and returned as fragments per kilobase of transcript per million mapped reads values, which means that they have been normalized also by the molecule size. Analyses of enriched pathways and gene annotations were performed using Ingenuity Pathway Analysis. To exclude false positives among the enriched genes that were caused by empty input, we only considered transcripts for which sufficient reads were detected in the input samples.

RNA extraction and quantitative RT-PCR

The immunoprecipitated RNA was extracted by incubating the beads with 10% SDS and 100 µg proteinase K (Promega) followed by phenol/chloroform/isoamyl and acid/chloroform extraction (ToTALLY RNA kit; Life Technologies). Precipitation of RNA was achieved by addition of isopropanol and GlycoBlue (Life Technologies) at −20°C. RNA was reverse transcribed with SuperScript First-Strand Synthesis System (Life Technologies) with oligo(dT) according to manufacturer's manual. Real-time PCR was performed with SYBR green (Life Technologies). Each reaction was performed in triplicate, and at least three biological replicates were performed. Primers used are listed in the Table S2. The fold enrichment was calculated with the formula $2^{(-DDCt)}$.

In vitro translation assay

Cells were primed in medium containing DMEM, L-glutamine, pyruvate, nonessential amino acids, dialyzed serum (Life Technologies), and penicillin-streptomycin for 15 min at 37°C. Cells were metabolically labeled in medium containing 50 µCi [^{35}S]methionine/cysteine (Hartmann Analytic). For the negative control, 100 µg/ml cycloheximide was added to the medium. Cells were collected at different time points, lysed in buffer containing 50 mM Tris-HCl, pH 7.4, 150 mM NaCl, 1 mM EDTA, pH 8, 1% IGEPAL CA-630, 0.25% sodium deoxycholate, and protease inhibitor cocktail. The proteins were resolved by SDS-PAGE and transferred to polyvinylidene difluoride membranes (VWR International) that were then exposed to x-ray film.

Statistical analysis

Statistical analysis for graphs was performed using a paired Student's *t* test. Error bars show standard errors of the mean.

Online supplemental material

Fig. S1 shows the domain structure of CLUH, the alignment between Clu domain in different species, and the list of the first 100 genes co-regulated with *Cluh*. Fig. S2 shows additional immunofluorescence analysis of CLUH. Fig. S3 shows results obtained after silencing of *Cluh* in NSC34 cells. Table S1 shows RIP-seq library statistics. Table S2 contains sequences of primers used in this study. Table S3 shows transcripts enriched with FC > 5 and P < 0.01 in CLUH-RIP versus IgG-RIP experiments and is provided online as an Excel (Microsoft) file. Table S4 shows transcripts enriched with FC > 5 and P < 0.01 in CLUH-RIP versus HeLa input mRNA and is provided online as an Excel file. Table S5 displays a comparison between the two types of analysis and is provided online as an Excel file. Online supplemental material is available at http://www.jcb.org/cgi/content/full/jcb.201403129/DC1.

The authors are grateful to Niels Gehring and members of his laboratory for helpful discussion and assistance with CLIP experiments, to Luke Tain and Ricarda Richter-Dennerlein for help with polysome profiling, to Teresa Corona for support in generation of *Cluh* KO MEFs, to Danilo Licastro for discussion about RNA sequencing data, and to Günter Rappl and the Central Cell Sorting Facility at the Center for Molecular Medicine.

This study was supported by a grant from the Deutsche Forschungsgemeinschaft to E.I. Rugarli (RU1653/2-1).

The authors declare no competing financial interests.

Submitted: 28 March 2014
Accepted: 18 September 2014

References

Anders, S., and W. Huber. 2010. Differential expression analysis for sequence count data. *Genome Biol.* 11:R106. http://dx.doi.org/10.1186/gb-2010-11-10-r106

Barrett, T., D.B. Troup, S.E. Wilhite, P. Ledoux, D. Rudnev, C. Evangelista, I.F. Kim, A. Soboleva, M. Tomashevsky, and R. Edgar. 2007. NCBI GEO: mining tens of millions of expression profiles—database and tools update. *Nucleic Acids Res.* 35(Suppl. 1):D760–D765. http://dx.doi.org/10.1093/nar/gkl887

Cappelletti, G., M.G. Maggioni, G. Tedeschi, and R. Maci. 2003. Protein tyrosine nitration is triggered by nerve growth factor during neuronal differentiation of PC12 cells. *Exp. Cell Res.* 288:9–20. http://dx.doi.org/10.1016/S0014-4827(03)00209-X

Cashman, N.R., H.D. Durham, J.K. Blusztajn, K. Oda, T. Tabira, I.T. Shaw, S. Dahrouge, and J.P. Antel. 1992. Neuroblastoma x spinal cord (NSC) hybrid cell lines resemble developing motor neurons. *Dev. Dyn.* 194:209–221. http://dx.doi.org/10.1002/aja.1001940306

Castello, A., B. Fischer, K. Eichelbaum, R. Horos, B.M. Beckmann, C. Strein, N.E. Davey, D.T. Humphreys, T. Preiss, L.M. Steinmetz, et al. 2012. Insights into RNA biology from an atlas of mammalian mRNA-binding proteins. *Cell*. 149:1393–1406. http://dx.doi.org/10.1016/j.cell.2012.04.031

Cho, K.I., Y. Cai, H. Yi, A. Yeh, A. Aslanukov, and P.A. Ferreira. 2007. Association of the kinesin-binding domain of RanBP2 to KIF5B and KIF5C determines mitochondria localization and function. *Traffic*. 8:1722–1735. http://dx.doi.org/10.1111/j.1600-0854.2007.00647.x

Clark, I.E., M.W. Dodson, C. Jiang, J.H. Cao, J.R. Huh, J.H. Seol, S.J. Yoo, B.A. Hay, and M. Guo. 2006. *Drosophila* pink1 is required for mitochondrial function and interacts genetically with parkin. *Nature*. 441:1162–1166. http://dx.doi.org/10.1038/nature04779

Cox, R.T., and A.C. Spradling. 2009. Clueless, a conserved *Drosophila* gene required for mitochondrial subcellular localization, interacts genetically with parkin. *Dis. Model. Mech.* 2:490–499. http://dx.doi.org/10.1242/dmm.002378

Dagda, R.K., S.J. Cherra III, S.M. Kulich, A. Tandon, D. Park, and C.T. Chu. 2009. Loss of PINK1 function promotes mitophagy through effects on oxidative stress and mitochondrial fission. *J. Biol. Chem.* 284:13843–13855. http://dx.doi.org/10.1074/jbc.M808515200

Devaux, F., G. Lelandais, M. Garcia, S. Goussard, and C. Jacq. 2010. Post-transcriptional control of mitochondrial biogenesis: spatio-temporal regulation of the protein import process. *FEBS Lett.* 584:4273–4279. http://dx.doi.org/10.1016/j.febslet.2010.09.030

Ferreirinha, F., A. Quattrini, M. Pirozzi, V. Valsecchi, G. Dina, V. Broccoli, A. Auricchio, F. Piemonte, G. Tozzi, L. Gaeta, et al. 2004. Axonal degeneration in paraplegin-deficient mice is associated with abnormal mitochondria and impairment of axonal transport. *J. Clin. Invest.* 113:231–242. http://dx.doi.org/10.1172/JCI200420138

Fields, S.D., M.N. Conrad, and M. Clarke. 1998. The *S. cerevisiae* CLU1 and *D. discoideum* cluA genes are functional homologues that influence mitochondrial morphology and distribution. *J. Cell Sci.* 111:1717–1727.

Fields, S.D., Q. Arana, J. Heuser, and M. Clarke. 2002. Mitochondrial membrane dynamics are altered in cluA- mutants of *Dictyostelium*. *J. Muscle Res. Cell Motil.* 23:829–838. http://dx.doi.org/10.1023/A:1024492031696

Gennarino, V.A., M. Sardiello, M. Mutarelli, G. Dharmalingam, V. Maselli, G. Lago, and S. Banfi. 2011. HOCTAR database: a unique resource for microRNA target prediction. *Gene*. 480:51–58. http://dx.doi.org/10.1016/j.gene.2011.03.005

Huang, D.W., B.T. Sherman, and R.A. Lempicki. 2009. Systematic and integrative analysis of large gene lists using DAVID bioinformatics resources. *Nat. Protoc.* 4:44–57. http://dx.doi.org/10.1038/nprot.2008.211

Jensen, K.B., and R.B. Darnell. 2008. CLIP: crosslinking and immunoprecipitation of in vivo RNA targets of RNA-binding proteins. *Methods Mol. Biol.* 488:85–98. http://dx.doi.org/10.1007/978-1-60327-475-3_6

Kim, D., G. Pertea, C. Trapnell, H. Pimentel, R. Kelley, and S.L. Salzberg. 2013. TopHat2: accurate alignment of transcriptomes in the presence of insertions, deletions and gene fusions. *Genome Biol.* 14:R36. http://dx.doi.org/10.1186/gb-2013-14-4-r36

Koppen, M., M.D. Metodiev, G. Casari, E.I. Rugarli, and T. Langer. 2007. Variable and tissue-specific subunit composition of mitochondrial m-AAA protease complexes linked to hereditary spastic paraplegia. *Mol. Cell. Biol.* 27:758–767. http://dx.doi.org/10.1128/MCB.01470-06

Lee, J.Y., Y. Nagano, J.P. Taylor, K.L. Lim, and T.P. Yao. 2010. Disease-causing mutations in parkin impair mitochondrial ubiquitination, aggregation, and HDAC6-dependent mitophagy. *J. Cell Biol.* 189:671–679. http://dx.doi.org/10.1083/jcb.201001039

Logan, D.C., I. Scott, and A.K. Tobin. 2003. The genetic control of plant mitochondrial morphology and dynamics. *Plant J.* 36:500–509. http://dx.doi.org/10.1046/j.1365-313X.2003.01894.x

Lopes, C.T., M. Franz, F. Kazi, S.L. Donaldson, Q. Morris, and G.D. Bader. 2010. Cytoscape Web: an interactive web-based network browser. *Bioinformatics*. 26:2347–2348. http://dx.doi.org/10.1093/bioinformatics/btq430

Marc, P., A. Margeot, F. Devaux, C. Blugeon, M. Corral-Debrinski, and C. Jacq. 2002. Genome-wide analysis of mRNAs targeted to yeast mitochondria. *EMBO Rep.* 3:159–164. http://dx.doi.org/10.1093/embo-reports/kvf025

Margeot, A., C. Blugeon, J. Sylvestre, S. Vialette, C. Jacq, and M. Corral-Debrinski. 2002. In *Saccharomyces cerevisiae*, ATP2 mRNA sorting to the vicinity of mitochondria is essential for respiratory function. *EMBO J.* 21:6893–6904. http://dx.doi.org/10.1093/emboj/cdf690

Martin, K.C., and A. Ephrussi. 2009. mRNA localization: gene expression in the spatial dimension. *Cell*. 136:719–730. http://dx.doi.org/10.1016/j.cell.2009.01.044

Matsumoto, S., T. Uchiumi, T. Saito, M. Yagi, S. Takazaki, T. Kanki, and D. Kang. 2012. Localization of mRNAs encoding human mitochondrial oxidative phosphorylation proteins. *Mitochondrion*. 12:391–398. http://dx.doi.org/10.1016/j.mito.2012.02.004

Mitchell, S.F., S. Jain, M. She, and R. Parker. 2013. Global analysis of yeast mRNPs. *Nat. Struct. Mol. Biol.* 20:127–133. http://dx.doi.org/10.1038/nsmb.2468

Narendra, D.P., and R.J. Youle. 2011. Targeting mitochondrial dysfunction: role for PINK1 and Parkin in mitochondrial quality control. *Antioxid. Redox Signal.* 14:1929–1938. http://dx.doi.org/10.1089/ars.2010.3799

Nunnari, J., and A. Suomalainen. 2012. Mitochondria: in sickness and in health. *Cell*. 148:1145–1159. http://dx.doi.org/10.1016/j.cell.2012.02.035

Otto, H., C. Conz, P. Maier, T. Wölfle, C.K. Suzuki, P. Jenö, P. Rücknagel, J. Stahl, and S. Rospert. 2005. The chaperones MPP11 and Hsp70L1 form the mammalian ribosome-associated complex. *Proc. Natl. Acad. Sci. USA*. 102:10064–10069. http://dx.doi.org/10.1073/pnas.0504400102

Park, J., S.B. Lee, S. Lee, Y. Kim, S. Song, S. Kim, E. Bae, J. Kim, M. Shong, J.M. Kim, and J. Chung. 2006. Mitochondrial dysfunction in *Drosophila* PINK1 mutants is complemented by parkin. *Nature*. 441:1157–1161. http://dx.doi.org/10.1038/nature04788

Sardiello, M., M. Palmieri, A. di Ronza, D.L. Medina, M. Valenza, V.A. Gennarino, C. Di Malta, F. Donaudy, V. Embrione, R.S. Polishchuk, et al. 2009. A gene network regulating lysosomal biogenesis and function. *Science*. 325:473–477.

Sen, A., V.T. Damm, and R.T. Cox. 2013. *Drosophila* clueless is highly expressed in larval neuroblasts, affects mitochondrial localization and suppresses mitochondrial oxidative damage. *PLoS ONE*. 8:e54283. http://dx.doi.org/10.1371/journal.pone.0054283

Smirnova, E., L. Griparic, D.L. Shurland, and A.M. van der Bliek. 2001. Dynamin-related protein Drp1 is required for mitochondrial division in mammalian cells. *Mol. Biol. Cell*. 12:2245–2256. http://dx.doi.org/10.1091/mbc.12.8.2245

Song, W., F. Wang, M. Savini, A. Ake, A. di Ronza, M. Sardiello, and L. Segatori. 2013. TFEB regulates lysosomal proteostasis. *Hum. Mol. Genet.* 22:1994–2009. http://dx.doi.org/10.1093/hmg/ddt052

Subramanian, A., P. Tamayo, V.K. Mootha, S. Mukherjee, B.L. Ebert, M.A. Gillette, A. Paulovich, S.L. Pomeroy, T.R. Golub, E.S. Lander, and J.P. Mesirov. 2005. Gene set enrichment analysis: a knowledge-based approach for interpreting genome-wide expression profiles. *Proc. Natl. Acad. Sci. USA*. 102:15545–15550. http://dx.doi.org/10.1073/pnas.0506580102

Tanaka, Y., Y. Kanai, Y. Okada, S. Nonaka, S. Takeda, A. Harada, and N. Hirokawa. 1998. Targeted disruption of mouse conventional kinesin heavy chain, kif5B, results in abnormal perinuclear clustering of mitochondria. *Cell*. 93:1147–1158. http://dx.doi.org/10.1016/S0092-8674(00)81459-2

Trapnell, C., B.A. Williams, G. Pertea, A. Mortazavi, G. Kwan, M.J. van Baren, S.L. Salzberg, B.J. Wold, and L. Pachter. 2010. Transcript assembly and quantification by RNA-Seq reveals unannotated transcripts and isoform switching during cell differentiation. *Nat. Biotechnol.* 28:511–515. http://dx.doi.org/10.1038/nbt.1621

van Spronsen, M., M. Mikhaylova, J. Lipka, M.A. Schlager, D.J. van den Heuvel, M. Kuijpers, P.S. Wulf, N. Keijzer, J. Demmers, L.C. Kapitein, et al. 2013. TRAK/Milton motor-adaptor proteins steer mitochondrial trafficking to axons and dendrites. *Neuron*. 77:485–502. http://dx.doi.org/10.1016/j.neuron.2012.11.027

Vornlocher, H.P., P. Hanachi, S. Ribeiro, and J.W. Hershey. 1999. A 110-kilodalton subunit of translation initiation factor eIF3 and an associated 135-kilodalton protein are encoded by the *Saccharomyces cerevisiae* TIF32 and TIF31 genes. *J. Biol. Chem.* 274:16802–16812. http://dx.doi.org/10.1074/jbc.274.24.16802

Wakabayashi, J., Z. Zhang, N. Wakabayashi, Y. Tamura, M. Fukaya, T.W. Kensler, M. Iijima, and H. Sesaki. 2009. The dynamin-related GTPase Drp1 is required for embryonic and brain development in mice. *J. Cell Biol.* 186:805–816. http://dx.doi.org/10.1083/jcb.200903065

Zhu, Q., D. Hulen, T. Liu, and M. Clarke. 1997. The cluA- mutant of *Dictyostelium* identifies a novel class of proteins required for dispersion of mitochondria. *Proc. Natl. Acad. Sci. USA*. 94:7308–7313. http://dx.doi.org/10.1073/pnas.94.14.7308